ASTRONOMY
AND
ASTROPHYSICS

Distant clusters of galaxies: X-ray properties and their relations

Sabine Schindler

Astrophysics Research Institute, Liverpool John Moores University, Twelve Quays House, Egerton Wharf, Birkenhead CH41 1LD, UK
(sas@staru1.livjm.ac.uk)

Abstract. We investigate the evolution of clusters of galaxies in a sample of distant clusters with redshifts between 0.3 and 1.0. We show the abilities and limitations of combined ROSAT and ASCA data to draw cosmological conclusions. For the first time bolometric luminosities, masses, gas masses, gas mass fractions, and iron masses are derived in such a distant sample in a consistent way. We compare these quantities with the corresponding quantities in nearby samples. Furthermore, we analyse relations between these quantities and the gas temperature, metallicity and the morphological parameters and compare them with relations in nearby samples. Fits to all relations with power law functions are given. We find relations between X-ray luminosity, temperature, mass, gas mass, core radius and β, similar to those found in nearby clusters. Furthermore, we find gas mass fractions increasing with radius, with the effect being stronger in less massive clusters. Within errors we find no evidence for evolution in any of the quantities nor in any of the relations. These results favour a low Ω universe, but without strong constraints. We point out how promising the next generation of X-ray satellites XMM, CHANDRA and ASTRO-E are for cosmological studies with clusters. From the new observations primarily two measurements are required: detection of more distant clusters and measurements of the spectral and spatial parameters with much higher precision.

Key words: galaxies: clusters: general – galaxies: intergalactic medium – cosmology: observations – cosmology: dark matter – X-rays: galaxies

1. Introduction

Distant clusters of galaxies provide important diagnostics for cosmology. They are the largest bound systems in the universe and as such can be used to test theories of the origin and the evolution of structure. Different cosmological models predict different relations between quantities obtainable from X-ray observations like the bolometric X-ray luminosity, the intra-cluster gas temperature, the total mass and the gas mass (e.g. Cavaliere et al. 1998b). A different evolution of these relations is predicted as well by different theories (see e.g. Bower 1997; Voit & Donahue 1998). The evolution of the cluster mass and the related quantity temperature depend e.g. sensitively on the cosmological parameters Ω and Λ (see e.g. Oukbir & Blanchard 1992; Cen & Ostriker 1994). Even the amount of dispersion in relations can reflect different cluster formation epochs (Scharf & Mushotzky 1997). Deviations from theoretical scaling relations (e.g. Kaiser 1986) can give useful insights into physical processes going on in clusters.

The differences in observables predicted by cosmological theories are becoming larger and larger with increasing redshift. Tests of theories are therefore most powerful, when clusters with the largest possible redshifts are used.

In this paper we analyse relations between the X-ray quantities of a sample of distant clusters ($z = 0.3$–1.0) and the evolution of these quantities by comparing them with the corresponding nearby results. Most relations are well measured for nearby clusters (e.g. the $L_X - T$ relation: Arnaud & Evrard 1999; Allen & Fabian 1998; Markevitch 1998, Reiprich 1998). The reasons why only few attempts have been made to determine X-ray relations in medium distant and distant clusters (e.g. Mushotzky & Scharf 1997), despite their importance to constrain cosmological models, are the large uncertainties in the measurements and the paucity of clusters found at high redshifts.

The sample used in this paper consists of all clusters at $z > 0.5$ with measured ASCA temperature and measured morphological parameters from ROSAT/HRI observations, complemented with 5 clusters fulfilling the same criteria within the redshift range $0.3 < z < 0.5$. No scaling relations are used, but for the first time in such a distant sample all quantities are derived directly from the measured parameters: temperature, countrate or luminosity in the ROSAT band, metallicity and morphological parameters. Masses and bolometric luminosities are calculated in a consistent way and masses are determined within equivalent volumes. Unlike our analysis, which compares comprehensively all derivable quantities, previous studies of cluster samples up to a redshift of 1 showed only few relations of directly measured quantities.

We demonstrate what the abilities and limitations of cosmological studies with distant clusters are when using a combination of the best X-ray data available today, spatially resolved data from the ROSAT/HRI (Trümper 1983) and X-ray spectra from ASCA (Tanaka et al. 1994). We show that with these data one sees similar relations as for nearby clusters, but of course

Table 1. X-ray quantities as measured from ROSAT/HRI and ASCA observations. The clusters (Column 1) are ordered according to redshift (Column 2). Columns (3), (4) and (5) list the bolometric X-ray luminosity, the metallicity in solar units and the temperature, respectively. In Columns (6), (7) and (8) the fit parameters of the β model are shown, central surface brightness, core radius r_c and the slope β. S_0 is in units of 10^{-2} ROSAT/HRI counts/s/$\square'$. Columns (8) and (9) give the total number of source counts in the ROSAT observation and the radius out to which the X-ray emission could be traced. Column. (10) denotes the references: (a) Mushotzky & Loewenstein 1997, (b) Mushotzky & Scharf 1997, (c) Neumann & Schindler 1999, (d) Schindler & Wambsganss 1997, (e) Ota et al. 1998, (f) Schindler et al. 1998, (g) Schindler et al. 1997, (h) Neumann 1999, (i) Neumann & Böhringer 1997, (j) Hughes & Birkinshaw 1998, (k) Donahue 1996, (l) Hattori et al. 1998, (m) Gioia et al. 1999, (n) Donahue et al. 1998, (o) Hattori et al. 1997

cluster	z	$L_{X,bol}$ $(10^{45}$ erg/s)	m (solar)	T (keV)	S_0	r_c (kpc)	β	source counts	r_{tot} (Mpc)	ref.
AC118	0.31	6.6	0.23 ± 0.09	$9.3^{+4.2}$	1.5	370 ± 40	0.63 ± 0.4	5300	2.1	a,b,c
Cl0500-24	0.32	0.6	0.0–1.5	$7.2^{+3.8}_{-1.8}$	0.8	30^{+470}_{-30}	$0.4^{+0.6}_{-0.1}$	440	0.9	d,e
Cl0939+4713	0.41	1.6	$0.22^{+0.24}_{-0.22}$	$7.6^{+2.8}_{-1.6}$	0.79	66^{+90}_{-47}	$0.36^{+0.9}_{-0.7}$	1100	1.0	f
RXJ1347-1145	0.45	21.	0.33 ± 0.10	$9.3^{+1.1}_{-1.0}$	61.	57 ± 12	0.57 ± 0.04	2200	1.7	g
3C295	0.46	2.6	-	$7.1^{+2.2}_{-1.3}$	33.	26 ± 16	0.52 ± 0.07	680	0.8	b,h
Cl0016+16	0.55	5.2	$0.07^{+0.11}_{-0.07}$	$7.6^{+0.7}_{-0.6}$	1.6	283^{+59}_{-48}	$0.68^{+0.10}_{-0.07}$	3700	1.5	i,j
MS0451-0305	0.55	7.0	$0.15^{+0.11}_{-0.12}$	10.4 ± 1.2	2.2	256^{+69}_{-53}	$0.68^{+0.13}_{-0.09}$	1400	1.6	k
Cl2236-04	0.55	1.5	$0.0^{+0.38}_{-0.0}$	$6.2^{+2.6}_{-1.7}$	3.9	66^{+41}_{-27}	$0.53^{+0.18}_{-0.09}$	480	0.6	l
RXJ1716+6708	0.81	1.4	$0.43^{+0.25}_{-0.21}$	$5.7^{+1.3}_{-0.6}$	0.85	56 ± 50	$0.42^{+0.14}_{-0.09}$	790	1.0	m
MS1054-0321	0.83	7.1	0.0–0.22	$12.3^{+3.1}_{-2.2}$	0.59	≈ 500	0.7–1.0	1100	$\gtrsim 0.5$	n
AXJ2019+112	1.01	1.1	$1.7^{+1.25}_{-0.74}$	$8.6^{+4.2}_{-3.0}$	0.33	≈ 150	≈ 0.9	76	0.5	o

with much less accuracy. For solid cosmological conclusions we have to wait for the new missions XMM, CHANDRA and ASTRO-E with their much enhanced collecting area, spatial and spectral resolution.

Other tests for cosmological models would be the investigation of the evolution of the luminosity function or the temperature function (see e.g. Burke et al. 1997; Henry 1997) or using the distribution of clusters to determine the correlation function (e.g. Mo et al. 1996; Guzzo et al. 1999). For these tests the selection function of the sample must be known very well. As the selection function for the sample in this paper is completely unknown, we make no attempt to determine any of these functions.

The paper is organised as follows. After a description of the data sources and analysis methods (Sect. 2) we show various relations in Sect. 3: relations of total mass, gas mass and iron mass (Sect. 3.1), relations with temperature (Sect. 3.2) and relations with the X-ray luminosity (Sect. 3.3). Finally, Sect. 4 gives our summary and conclusions. Throughout this paper we use $H_0 = 50$ km/s/Mpc and $q_0 = 0.5$.

2. Data

We select the most distant clusters with published ASCA temperatures which were also observed with the ROSAT/HRI (see Table 1). The sample includes all the clusters meeting this criterion above a redshift of $z = 0.5$. These are 6 clusters. For the redshift range $z = 0.3$–0.5 only a few clusters of the many observed ones were selected. Including more of these low redshift clusters would have resulted in a sample heavily dominated by clusters at redshifts $z = 0.3$–0.5 which would have made it use-

less for a study of the evolution of clusters. As all the clusters in the sample above a redshift of $z = 0.5$ show the gravitational lensing effect we chose 5 clusters in the redshift range $z = 0.3$–0.5, which show a gravitational lensing signal as well as meet the above mentioned criteria. In total the sample consists of 11 clusters.

Obviously, the sample is not complete in any sense, therefore no analyses of distribution functions can be made with it. But the analyses of correlations between the different quantities should not be affected by the incompleteness because the clusters were detected by only ONE criterion, e.g. high X-ray luminosity or high mass in case of the lensing cluster AXJ2019+112. All other quantities, apart from this one that was used to detect the cluster, are therefore not biased in any way. Therefore the unknown selection function can hardly influence the results on correlations.

In literature different methods are used to determine the bolometric luminosity and we found considerable variations from author to author. In our analysis we derive the bolometric luminosity in a uniform way for all the clusters with the ROSAT data analysis software EXSAS. We start from the ROSAT/HRI countrate. Only for the clusters AC118 and Cl0016+16, for which also ROSAT/PSPC observations are available, we use the countrates from the ROSAT/PSPC observation as this is the more sensitive instrument and provides therefore a more accurate measurement of the luminosity. We use the temperature, metallicities and hydrogen column densities given in the publications listed in Table 1. The derived bolometric luminosities are listed there as well.

As the mass of a cluster is increasing with radius masses can only be compared when derived within equivalent volumes.

Table 2. Total mass, gas mass and gas mass fraction. The first and the second column give the cluster name and redshift, respectively. Column (3) denotes the radius r_{500} which comprises an overdensity of 500 over the critical density. Columns (4), (5) and (6) list the total mass, the gas mass and the gas mass fraction within r_{500}, respectively. In Columns (7), (8) and (9) the same quantities are listed for a radius $0.5 \times r_{500}$. The errors listed are only the errors coming from the uncertainty in the temperature measurement.

cluster	z	r_{500} (Mpc)	$M_{tot,500}$ ($10^{14} M_\odot$)	$M_{gas,500}$ ($10^{14} M_\odot$)	$f_{gas,500}$	$M_{tot,500/2}$ ($10^{14} M_\odot$)	$M_{gas,500/2}$ ($10^{14} M_\odot$)	$f_{gas,500/2}$
AC118	0.31	$1.35^{+0.25}_{-0.10}$	$8.1^{+3.7}_{-1.1}$	1.75	$0.22^{+0.04}_{-0.07}$	$3.3^{+1.5}_{-0.5}$	0.54	$0.16^{+0.03}_{-0.05}$
Cl0500-24	0.32	$0.97^{+0.23}_{-0.13}$	$3.0^{+1.6}_{-0.7}$	0.25	$0.08^{+0.03}_{-0.03}$	$1.5^{+0.8}_{-0.4}$	0.07	$0.05^{+0.02}_{-0.02}$
Cl0939+4713	0.41	$0.86^{+0.14}_{-0.10}$	$2.5^{+0.9}_{-0.5}$	0.44	$0.18^{+0.05}_{-0.05}$	$1.2^{+0.4}_{-0.3}$	0.11	$0.09^{+0.02}_{-0.02}$
RXJ1347-1145	0.45	$1.14^{+0.07}_{-0.04}$	$6.6^{+0.8}_{-0.7}$	2.20	$0.33^{+0.04}_{-0.04}$	$3.3^{+0.4}_{-0.4}$	0.85	$0.26^{+0.03}_{-0.03}$
3C295	0.46	$0.94^{+0.13}_{-0.09}$	$3.8^{+1.1}_{-0.7}$	0.59	$0.16^{+0.03}_{-0.03}$	$1.9^{+0.6}_{-0.4}$	0.21	$0.11^{+0.02}_{-0.03}$
Cl0016+16	0.55	$0.98^{+0.05}_{-0.04}$	$5.1^{+0.5}_{-0.4}$	1.31	$0.25^{+0.02}_{-0.02}$	$2.1^{+0.2}_{-0.2}$	0.42	$0.20^{+0.02}_{-0.02}$
MS0451-0305	0.55	$1.17^{+0.06}_{-0.08}$	$8.6^{+1.0}_{-1.0}$	1.68	$0.20^{+0.03}_{-0.02}$	$3.8^{+0.4}_{-0.4}$	0.60	$0.16^{+0.02}_{-0.02}$
Cl2236-04	0.55	$0.81^{+0.16}_{-0.12}$	$2.9^{+1.2}_{-0.8}$	0.54	$0.19^{+0.07}_{-0.06}$	$1.4^{+0.6}_{-0.4}$	0.19	$0.14^{+0.05}_{-0.04}$
RXJ1716+6708	0.81	$0.55^{+0.06}_{-0.03}$	$1.4^{+0.3}_{-0.1}$	0.23	$0.16^{+0.02}_{-0.03}$	$0.7^{+0.2}_{-0.1}$	0.06	$0.09^{+0.01}_{-0.02}$
MS1054-0321	0.83	$1.02^{+0.14}_{-0.12}$	$9.4^{+2.4}_{-1.7}$	1.61	$0.17^{+0.04}_{-0.03}$	$3.0^{+0.8}_{-0.5}$	0.46	$0.15^{+0.03}_{-0.03}$
AXJ2019+112	1.01	$0.84^{+0.18}_{-0.17}$	$6.9^{+3.4}_{-2.4}$	0.18	$0.03^{+0.01}_{-0.01}$	$3.2^{+1.6}_{-1.1}$	0.93	$0.03^{+0.02}_{-0.01}$

The masses in literature are usually determined at arbitrary radii and are therefore not directly comparable. We determine all the masses at a radius r_{500} which encompasses a density $500 \times$ the critical density $\rho_c(z) = 3H_0^2/(8\pi G)(1+z)^3$ (see Table 2). A comparison with the X-ray extent of the clusters (see Table 1) shows that in most clusters the X-ray emission could be traced out to r_{500}. For the determination of the radial dependence of the gas mass fraction we determine additionally the mass at the radius $0.5 \times r_{500}$.

To deproject the two-dimensional X-ray emission to three-dimensional densities and masses we use the β model (Cavaliere & Fusco-Femiano 1976; Jones & Forman 1984)

$$S(r) = S_0 \left(1 + \left(\frac{r}{r_c}\right)^2\right)^{-3\beta+1/2}, \tag{1}$$

where $S(r)$ is the surface brightness at distance r, S_0 is the central surface brightness, r_c is the core radius, and β is the slope. We use only β-models fitted to ROSAT/HRI data for all clusters. A comparison with β-model parameters of ROSAT/PSPC data shows that the ROSAT/PSPC parameters are systematically larger for these high redshift clusters, even when they are deconvolved with the point spread function. While for nearby clusters the ROSAT/PSPC data give a good estimate of the mass, for clusters at high redshifts the point spread function distorts the profile, i.e. it flattens the profile in the centre. The result is a β-model fit with a larger core radius in the ROSAT/PSPC data and this is compensated by a larger β. This larger β yields a steeper slope in the outer parts and thus results in a larger mass estimate at the radius considered here. This effect can overestimate the mass for high redshift clusters up to almost 50% (e.g. in Cl0016+16 using fit parameters by Neumann & Böhringer (1997) and Hughes & Birkinshaw (1998) or in Cl0939+4713 using the parameters of Schindler & Wambsganss (1996) and Schindler et al. (1998)). The difference depends of course on the radius where the mass is determined. Compared to this the effect of the point spread function of the ROSAT/HRI on the mass is small ($\lesssim 10\%$).

With the assumption of hydrostatic equilibrium, the integrated total mass can be calculated from the equation

$$M(r) = \frac{-kr}{\mu m_p G} T \left(\frac{d\ln\rho}{d\ln r} + \frac{d\ln T}{d\ln r}\right), \tag{2}$$

where ρ and T are the density and the temperature of the intracluster gas, and r, k, μ, m_p, and G are the radius, the Boltzmann constant, the molecular weight, the proton mass, and the gravitational constant, respectively. For distant clusters it is very difficult to measure a temperature gradient. But in any case the density gradient is dominating the brackets in Eq. 2. Therefore we assume that the clusters are isothermal with the temperatures listed in Table 1. The resulting masses and gas masses within r_{500} are listed in Table 2. The listed errors on the mass are only the errors coming from the uncertainty in the temperature. The true mass uncertainties are larger because of the additional uncertainties coming from deviations from spherical symmetry, deviations from hydrostatic equilibrium and projection effects (about 15%; see Evrard et al. 1996; Schindler 1996), but these are hard to quantify for each cluster individually. Therefore we only show the errors from the temperature but keep in mind that the true errors are larger.

For the luminosity an error of 10% and for the gas mass an error of 15% is used to derive the error on the power law index. Only for AXJ2019+112 much larger errors, 33% and 50%, respectively, are used. These errors are estimated to include the uncertainties in the conversion of luminosities in the ROSAT band to bolometric luminosities, uncertainties in the background determination and possible contributions of AGNs or background quasars. The AGN contribution is assumed to be small. For the cluster 3C295, which hosts a luminous radio source and an AGN contribution to the X-ray emission could

be expected, a thorough spatial analysis of the ROSAT/HRI data was done, and it was concluded that there is no X-ray point source present in the cluster (Neumann 1999). For the other clusters only minor contributions are expected as the mean AGN luminosity in the ROSAT band is only about 5×10^{43} erg/s (Grupe et al. 1998). Furthermore, in none of the spectra a strong nonthermal component was required to fit the data. In Cl0939+472 the X-ray contribution of a background quasar could clearly be identified and was subtracted from the luminosity of the cluster (Schindler et al. 1998). The contribution to the count rate was less than three percent. Therefore, if there are background quasars in other clusters, which were not identified, we expect that their contribution is even less than three percent. Another possible contamination of the luminosity can come from cooling flows (Fabian et al. 1994). As will be seen later this is very obvious for the cluster RXJ1347-1145 with its very strong cooling flow of $\gtrsim 3000 M_\odot$/year (Schindler et al. 1997). Unfortunately, it is very difficult in distant clusters to separate cluster emission from cooling flow emission as many assumptions have to be made and only few observational data are available. Therefore we do not make an attempt to correct for the cooling flow emission, but exclude the luminosity of RXJ1347-1145 for the correlation analysis as will be shown later. For the other clusters in the sample (including 3C295 which has a cooling flow 4–9 times weaker than the one in RXJ1347-1145 (see Neumann 1999)) the cooling flow contribution to the luminosity is probably small because for none of them a deviation from the expected luminosity is visible.

We fit power law functions to all relations for which the linear correlation coefficient predicts a probability of more than 95% that the data are correlated. The fits take into account the errors in both axes. Note that for the total masses we use only the errors induced by the uncertainty of the temperature measurement as listed in Table 2. Increasing the errors on all data points by a fixed factor on both axes yields the same best fit results only the errors on the fit parameters would be larger. Therefore the errors on the power law indices are strictly speaking only lower limits.

Finally, we list some details about particular clusters. For AC118 two different temperature measurement are published: 9.3 keV (Mushotzky & Loewenstein 1997) and 12.1 keV (Mushotzky & Scharf 1997). We use the former value, but assume a large error which comprises also the error range of Mushotzky & Scharf (1997). For Cl0016+16 two slightly different temperatures and metallicities are published by Furuzawa et al. (1998) and Hughes & Birkinshaw (1998). We use the latter ones. For RXJ1347-1145 we use in addition to the data set used in Schindler et al. (1997) two more data sets observed in the meantime resulting in slightly different β-model parameters. No analysis of the MS0451-0305 ROSAT/HRI data is published, therefore we determine countrate and β-model parameters from the data in the archive. For two clusters with strong subclusters, AC118 and Cl0939+4713, the β-fit is centred on the main maximum and the region around the second maximum is neglected for the fit. As shown in Schindler (1996) this is a good way to obtain a reliable mass estimate. The β-model parameters of

Table 3. Symbols used for the various clusters in the figures

Symbol	Cluster
○	AC118
△	Cl0500-24
□	Cl0939+4713
⬡	RXJ1347-1145
☆	3C295
×	Cl0016+16
⟁	MS0451-0305
✳	Cl2236-04
●	RXJ1716+6708
▲	MS1054-0321
■	AXJ2019+112

MS1054-0321 are not well constrained (Donahue at al. 1998). We used the central value of their error range for $\beta = 0.85$ and estimate the error on the core radius to ± 200kpc.

3. Results

3.1. Relations of total mass, gas mass and iron mass

To test whether there is any dependence on redshift within our sample we plot various quantities versus redshift (Fig. 1). In this figure, as well as in all other following figures, each cluster is plotted with a different symbol (see Table 3). The open symbols (open circle, open triangle, open square and open hexagon) show the most nearby clusters of the sample, the starred and skeletal symbols (star, cross and asterisks) show the clusters at intermediate redshift and the filled symbols (filled circle, filled triangle and filled square) indicate the most distant clusters.

Fig. 1a shows the total mass and the gas mass, both determined within the radius r_{500} (see Table 2). Both quantities show a considerable scatter, but no trend with redshift. The total masses range from $1.4 \times 10^{14} M_\odot$ in RXJ1716+6708 to $9.4 \times 10^{14} M_\odot$ in MS1054-0321. The gas masses vary between $1.8 \times 10^{13} M_\odot$ (AXJ2019+112) and $2.2 \times 10^{14} M_\odot$ (RXJ1347-1145).

From the total mass and the gas mass we derive the gas mass fraction f_{gas} at r_{500} (Fig. 1b). Also in the gas mass fraction we see no clear trend with redshift (only AXJ2019+112 is an obvious outsider). This result does not confirm the trend of decreasing gas mass fractions by Tsuru et al. (1997). The mean value is $\langle f_{gas} \rangle = 0.18$, which is in agreement within the scatter with the values for nearby samples, e.g. Arnaud & Evrard (1999): $f_{gas} = 0.16$ and 0.20, respectively, Mohr et al. (1999): $f_{gas} = 0.21$ and Ettori & Fabian (1999): $f_{gas} = 0.17$. Therefore we conclude, that we do not see evolution in the gas mass fraction in these data. This result does not confirm the result by Ettori & Fabian (1999) where evolution of the gas mass fraction is found in a nearby sample.

We see large variations in the gas mass fraction of more than an order of magnitude between individual clusters, ranging from the exceptionally low fraction of 0.026 in AXJ2019+112 to 0.33
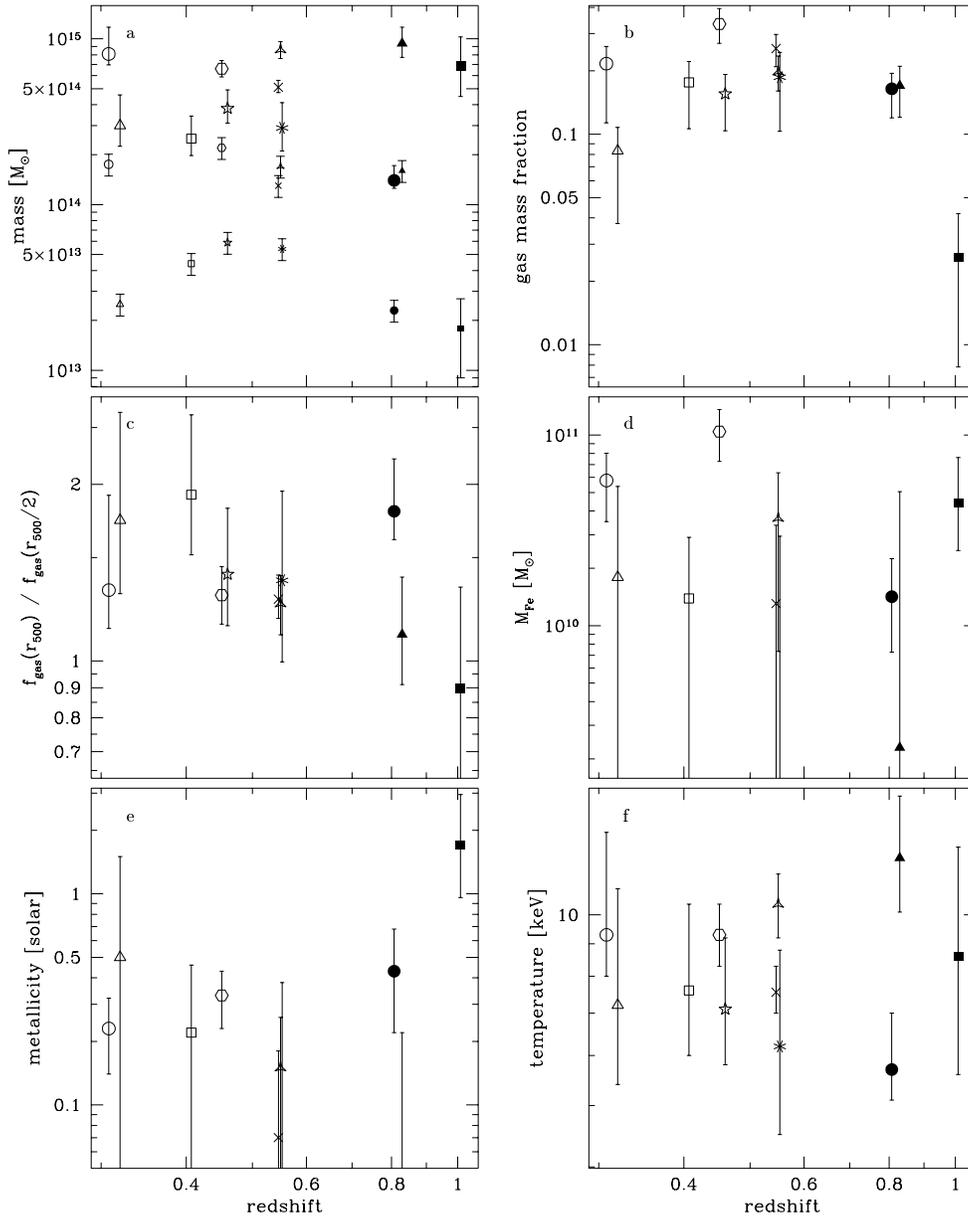
Fig. 1a–f. Various X-ray properties against redshift. **a** Gas and total mass. The large symbols show the total mass, the small symbols show the gas mass of the corresponding clusters. For explanation of the symbols see Table 3. **b** Gas mass fraction, **c** ratio of gas mass fractions at r_{500} and $r_{500}/2$ as a measure for the relative extent of the gas distribution, **d** iron mass in the intra-cluster gas, **e** metallicity, **f** temperature.

in RXJ1347-1145, very similar to what Ettori & Fabian (1999) and Reiprich (1998) found in nearby samples, but contradicting the result by Wu et al. (1999).

The gas mass fraction is not constant with radius. We compare the gas mass fraction at r_{500} with the gas mass fraction at $0.5 \times r_{500}$. The mean gas mass fraction at $0.5 \times r_{500}$ is 0.13, i.e. smaller than the mean of 0.18 at r_{500}. In Fig. 1c we show the ratio of these fractions E for the individual clusters. We see an increase of gas mass fraction with radius (i.e. $E > 1$) in all clusters apart from AXJ2019+112. The physical interpretation of E is the extent of the gas distribution relative to the dark matter extent. This means that in general the gas distribution is more extended than the dark matter, which is in agreement with the results for nearby cluster samples by David et al. (1995), Jones & Forman (1999), and Ettori & Fabian (1999). Obviously, cluster evolution is not completely a self-similar process, but physical

processes taking place in the gas must be taken into account, like e.g. energy input by supernovae, galactic winds or ram-pressure stripping (see e.g. Metzler & Evrard 1997; Cavaliere et al. 1998a). There is no trend of this relative gas extent with redshift.

Using the gas masses and the metallicities determined from ASCA observations (see Table 1) we can determine the iron mass in the intra-cluster gas. Unfortunately, the metallicities have large uncertainties and only for 5 clusters they are not compatible with zero, which makes it difficult to see any trends (see Fig. 1d). As far as one can see there is no dependence of the iron mass on redshift.

The lowest two panels of Fig. 1 show the metallicity and the temperature versus redshift. Also here no trend is visible within the sample. Within the error bars both distributions are consistent with a horizontal line. The same result for the temperature
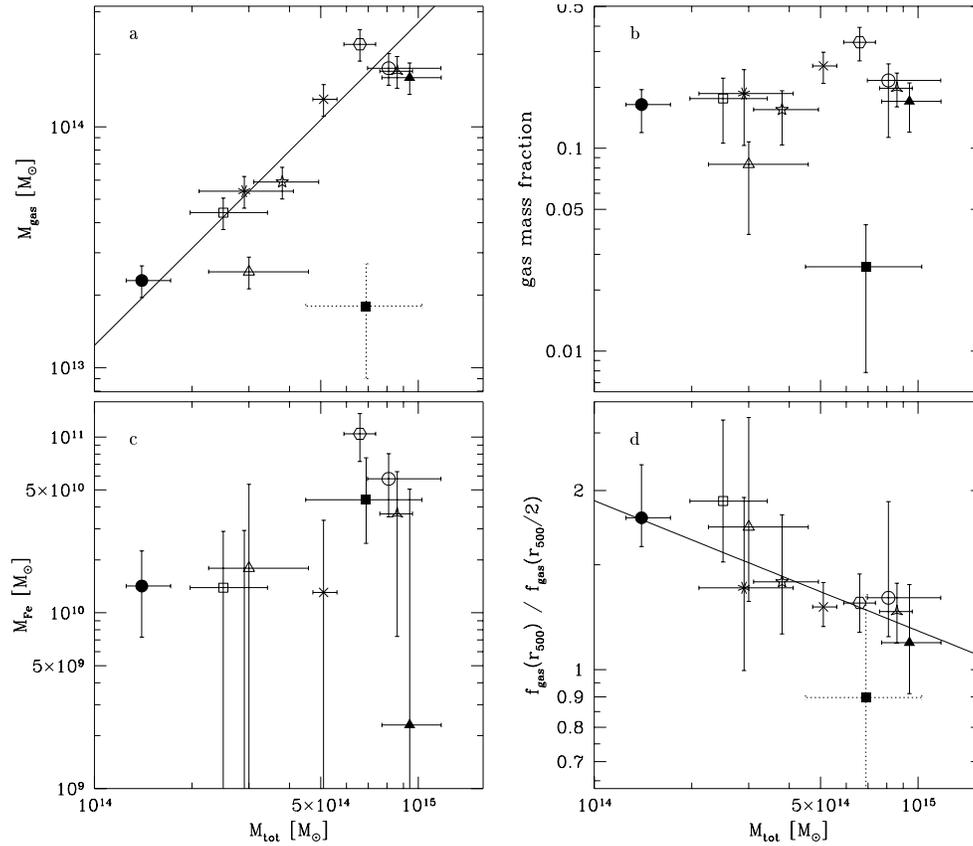
Fig. 2a–d. Various masses versus total mass. **a** Gas mass. The solid line is the best fit excluding AXJ2019+112 (filled square with dashed error bars). **b** The gas mass fraction is independent of the total mass. **c** Iron mass in the intra-cluster gas. **d** Ratio of gas mass fractions at r_{500} and $r_{500}/2$ as measure for the relative extent of the gas distribution. The solid line is again the best fit excluding AXJ2019+112.

was found for a medium redshift sample ($0.14 < z < 0.54$) by Mushotzky & Scharf (1997). Also for the metallicity the result is in agreement with the result for medium distant samples (Tsuru et al. 1996; Mushotzky & Loewenstein 1997) and with theoretical predictions by Martinelli et al. (1999). The mean value of the metallicity in our sample is $\langle m \rangle = 0.36$. Considering the large error this is in good agreement with iron abundances of nearby clusters $m = 0.2$–0.3 (Fukazawa et al. 1998).

In Fig. 2 we compare different masses with each other. A trend of an increasing gas mass with total mass which was found for nearby clusters by Arnaud & Evrard (1999) is also visible in our sample when omitting AXJ2019+112 (Fig. 2a). A fit without taking into account AXJ2019+112 yields

$$M_{gas,500} = 0.12\, M_{tot,500}^{(1.3\pm0.2)}. \tag{3}$$

$M_{gas,500}$ and $M_{tot,500}$ are in units of $10^{14} M_\odot$. Note that the error on the power law index in Eq. 3 and all following relations is probably even larger than indicated here, because we could not take into account all possible error sources.

Because the exponent in Eq. 3 is close to unity, we find basically no dependence of the gas mass fraction on the total mass (see Fig. 2b). Again AXJ2019+112 is lying clearly far away with a gas mass fraction an order of magnitude too low for its total mass.

In Fig. 2c the total mass is plotted versus the iron mass. Again the iron mass is very uncertain because of the large uncertainties in the metallicity measurements. One can see here a marginal trend of more massive clusters having more iron mass.

This can be explained easily. The gas mass is proportional to the total mass ($\approx$ constant gas mass fraction) while the metallicity is independent of the total mass. As the iron mass is a product of gas mass and metallicity, it must increase with increasing total mass. But because of the large errors on the data we do not attempt a fit through these data.
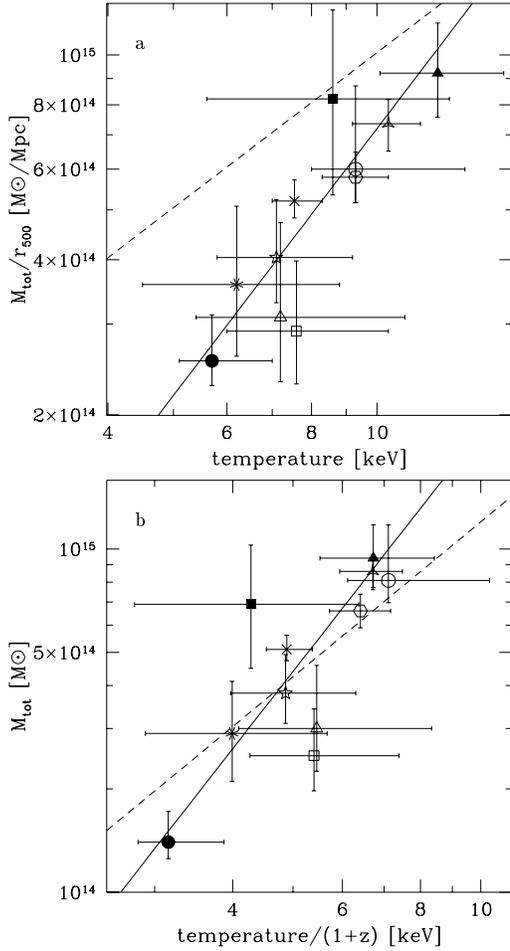
The relative extent E of the gas distribution with respect to the dark matter (expressed as the ratio of gas mass fractions at r_{500} and $0.5 \times r_{500}$) shows an interesting dependence on the total mass (Fig. 2d). Clusters with larger masses have smaller relative gas extents. A fit without taking into account AXJ2019+112 yields

$$E = f_{gas}(r_{500})/f_{gas}(r_{500}/2) = 1.9\, M_{tot,500}^{(-0.22\pm0.11)}, \tag{4}$$

with $M_{tot,500}$ in units of $10^{14} M_\odot$. A similar dependence of the relative gas extent on the total mass was confirmed by Reiprich (priv. comm.) for a nearby sample.

3.2. Mass – temperature relation

Assuming self-similarity and a velocity dispersion proportional to the X-ray temperature, the viral theorem provides a relation between total mass, radius and X-ray temperature: $M_{tot,500}/r_{500} \propto T$. We see this correlation in our data (see Fig. 3a). But the slope is different from unity which is the expected slope from virial considerations, although the expected slope is almost within the error. For comparison, in nearby lens-

Fig. 4. Temperature – r_{500} relation.

Fig. 3a and b. Mass – temperature relations. **a** The best fit curve is shown by the solid line. The dashed line is not a fit but the curve expected from virial considerations with the normalisation of Evrard et al. (1996). **b** Equivalent diagram with r being expressed by the definition of the overdensity contrast. For comparison, the dashed line shows again the slope expected from virial assumptions, here with an arbitrary normalisation.
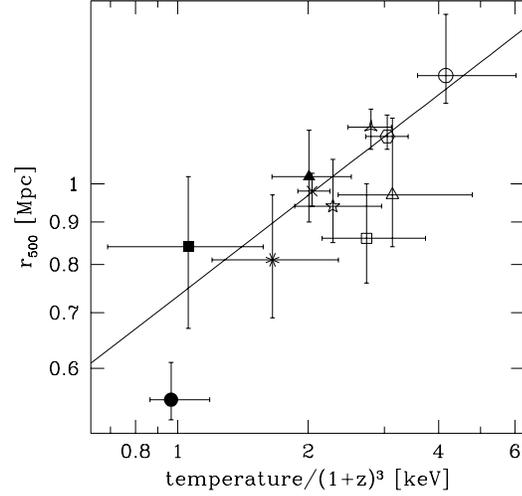
ing observations ($z = 0.17$–0.54) Hjorth et al. (1998) found good agreement with a slope of 1. Our best fit is

$$M_{tot,500}/r_{500} = 0.14\, T^{(1.7\pm0.6)}, \tag{5}$$

(compare solid and dashed line in Fig. 3a). $M_{tot,500}$ is in units of $10^{14} M_\odot$, r_{500} is in units of Mpc and T is in units of keV.

Equivalently, r_{500} can be expressed by the definition of the overdensity $r_{500} \propto M_{tot,500}^{1/3}/(1 + z)$ yielding the relation $M_{tot,500} \propto (T/(1 + z))^{3/2}$. For comparison with nearby clusters we plot also this relation (Fig. 3b). We find a trend of increasing mass with increasing $T/(1 + z)$. A fit taking into account the errors in the temperature and the error in the mass yields the following relation

$$M_{tot,500} = 0.10 \left(\frac{T}{1+z} \right)^{(2.3\pm0.8)}, \tag{6}$$

shown in Fig. 3b as solid line. $M_{tot,500}$ is again in units of $10^{14} M_\odot$ and T in units of keV. The slope is again steeper than the 1.5 expected from the virial theorem. For comparison we plot also a line with this slope in Fig. 3b. Obviously, the errors and the scatter are so large that no final conclusions can be drawn as the virial value is included in the errors. Also in nearby clusters slopes larger than 1.5 were found. Ettori & Fabian (1999) find in a sample of cluster with redshifts between 0.05 and 0.44 an exponent of 1.93 ± 0.09. Horner et al. (1999) find an exponent of 1.8–2.0 and Reiprich (1998) finds an exponent of 2.0.

Another way of putting the same relation is relating the radius to the temperature: $r_{500} \propto T^{1/2}/(1 + z)^{3/2}$. Of course, the relation is also visible in this way (see Fig. 4). The fit gives a slightly smaller slope than the expected 0.5, but 0.5 is well included in the error:

$$r_{500} = 0.73 \left(\frac{T}{(1+z)^3} \right)^{(0.40\pm0.24)}, \tag{7}$$

with r_{500} in Mpc and T in keV. Mohr & Evrard (1997) found also a radius – temperature relation for nearby clusters. But different from r_{500} they used the isophotal radius of the X-ray emission and found a larger slope of 0.93.

Furthermore, we test the relation of the gas mass and the gas mass fraction on the temperature. As expected from the gas mass – total mass relation, there is also a relation between gas mass and temperature (see Fig. 5a), in particular when the gas mass outsider AXJ2019+112 is removed. A fit without AXJ2019+112 yields

$$M_{gas,500} = 2.0 \times 10^{-4}\, T^{(4.1\pm1.5)}, \tag{8}$$

with $M_{gas,500}$ in units of $10^{14} M_\odot$ and T in keV. This correlation was also found in nearby clusters (Reiprich 1998; Jones & Forman 1999). For comparison, Reiprich (1998) finds an exponent of 2.9.

As expected from the non-correlation of gas mass fraction with the total mass, we find also no correlation between the gas mass fraction and the temperature (see Fig. 5b). This result is
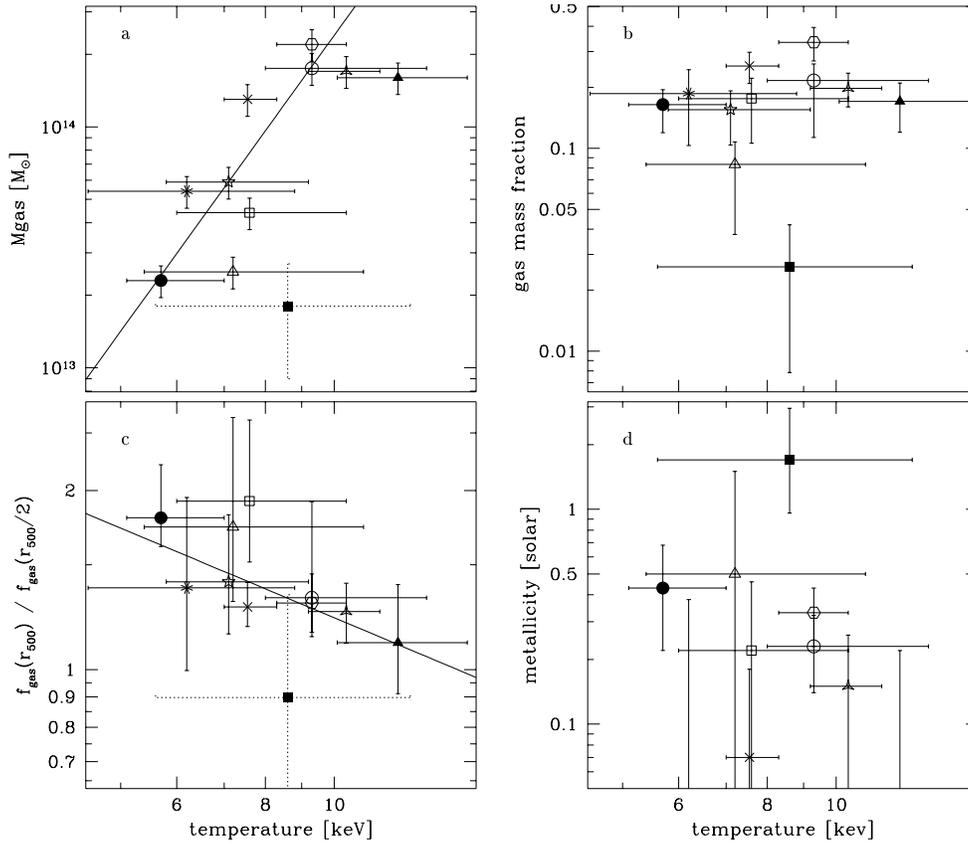
Fig. 5a–d. Various quantities versus the temperature. **a** Gas mass, **b** gas mass fraction, **c** ratio of gas mass fractions at r_{500} and $r_{500}/2$), **d** metallicity. AXJ2019+112 (solid square) is excluded in the fits.

in good agreement with Mohr et al. (1999). They find a mild dependence comparing low temperature clusters ($T < 5\,\mathrm{keV}$) with high temperature clusters ($T > 5\,\mathrm{keV}$). For the high temperature clusters alone, in which category all our clusters fall, they find no dependence.

We find an interesting correlation between the relative gas extent and the temperature (Fig. 5c), which is of course related to the dependence of the relative extent on the total mass, shown above. The extent of the gas relative to the extent of the dark matter tends to be larger in lower temperature clusters. Excluding again AXJ2019+112 one finds

$$E = f_{gas}(r_{500})/f_{gas}(r_{500}/2) = 3.9\,T^{(-0.50\pm0.34)},\qquad(9)$$
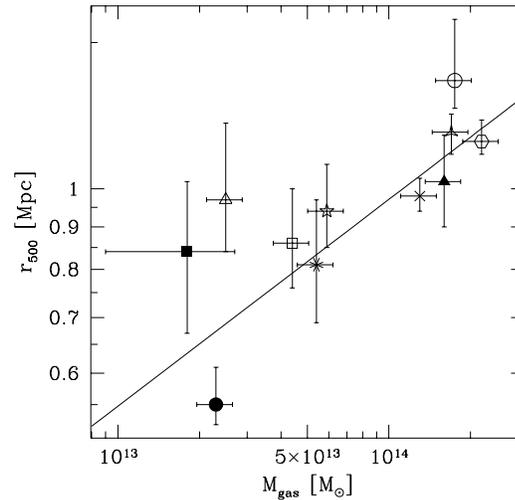
with the temperature in keV.

We see no correlation between temperature and metallicity in our sample (Fig. 5d) confirming the result by Tsuru et al. (1997).

As the definition of the overdensity contains a relation between total mass and radius, and there is also a relation between total mass and gas mass, we expect a relation between the gas mass and r_{500}, which is indeed visible in Fig. 6. A fit yields

$$r_{500} = 0.97\,M_{gas,500}^{(0.25\pm0.04)},\qquad(10)$$

with r_{500} in units of Mpc and $M_{gas,500}$ in $10^{14}M_{\odot}$.

Fig. 6. Gas mass – r_{500} relation.

3.3. Relations with the X-ray luminosity

The relation between the X-ray luminosity and the temperature, two directly observable quantities, is often used to compare gas and dark matter distribution in clusters, as the X-ray luminosity is connected with the gas while the temperature is related to the total mass of the cluster. Also we find in our data the well-known luminosity – temperature relation (see Fig. 7). RXJ1347-1145 is lying above the other clusters, which is expected because of
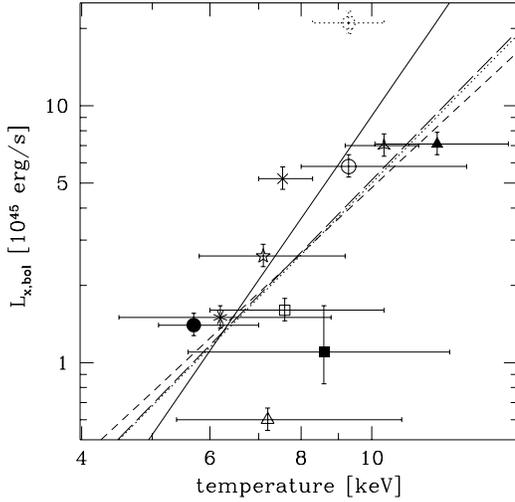
Fig. 7. Luminosity – temperature relation. The best fit which excludes RXJ1347-1145 (dotted hexagon) is indicated by a solid line. Some $L_X - T$ relations for nearby clusters are also shown: Arnaud & Evrard 1999 (dotted line), Allen & Fabian 1998 (long-dashed line) and Markevitch 1998 (short-dashed line). Apart from RXJ1347-1145 (dotted hexagon), which lies well above the other clusters because of the strong cooling flow, all other clusters are consistent with $L_X - T$ relations for nearby clusters: Arnaud & Evrard 1999 (dotted line), Allen & Fabian 1998 (long-dashed line) and Markevitch 1998 (short-dashed line). Our fit, excluding RXJ1347-1145 (dotted hexagon), is indicated by a solid line.

its very strong cooling flow (Fabian et al. 1994). Therefore it is excluded for the fit

$$L_{X,bol} = 6.9 \times 10^{-4} \, T^{(4.1 \pm 1.7)}, \tag{11}$$

with L_X in units of 10^{45} erg/s and T in keV. We find a larger slope than recently derived $L_X - T$ relations for nearby clusters (Arnaud & Evrard 1999: 2.9; Allen & Fabian 1998: 2.9; Markevitch 1998: 2.6; Jones & Forman 1999: 2.8) and for a sample including distant cluster but being heavily dominated by nearby clusters (Wu et al. 1999: 2.7), but the slopes for nearby clusters are still within the error. Some nearby $L_X - T$ relations are also shown in Fig. 7 for comparison. Introducing a term $(1 + z)^A$ (see Oukbir & Blanchard 1997) does not reduce the scatter of the data and does not improve the agreement with the nearby relations. This can be seen directly in Fig. 7 where the term $(1 + z)^A$ would shift the starred symbols slightly and the filled symbols considerably to the right. As these symbols lie on both sides of the fit curve, it would not help to reduce the scatter. Our conclusion from this is that we cannot see significant signs of evolution in the $L_X - T$ relation. The same conclusion was also drawn from medium distant samples by Tsuru et al. (1996) and Mushotzky & Scharf (1997) and from samples covering all redshifts up to $z = 1$ by Tsuru et al. (1997) and Sadat et al. (1998).

As expected from the correlations between mass–temperature and luminosity–temperature, the luminosity and the total mass show a correlation as well (see Fig. 8a). A fit with a power law (again excluding RXJ1347-1145) yields

$$M_{tot,500} = 1.8 \, L_{X,bol}^{(0.75 \pm 0.10)}, \tag{12}$$

($L_{X,bol}$ in units of 10^{45} erg/s, $M_{tot,500}$ in units of $10^{14} M_\odot$). For comparison, in a sample of 106 nearby clusters an exponent of 0.8 was found (Reiprich & Böhringer 1999).

The luminosity shows a tight correlation with the gas mass (see Fig. 8b)

$$M_{gas,500} = 0.29 \, L_{X,bol}^{(0.92 \pm 0.07)}, \tag{13}$$

($L_{X,bol}$ in units of 10^{45} erg/s, $M_{gas,500}$ in units of $10^{14} M_\odot$, RXJ1347-1145 excluded). As the X-ray emission is proportional to the square of the gas density this relation gives hints on the gas distribution. The small scatter in the above relation shows that the gas in these clusters has similar distributions, e.g. not different degrees of clumpiness.

This tight correlation of gas mass and luminosity was also found in a nearby sample by Jones & Forman (1999) although they measured the mass with a fixed radius of 1 Mpc. Our result is also in relative good agreement with the result for a nearby sample by Reiprich (1998) who used the luminosity in the ROSAT band (0.1–2.4 keV) and found a slope of 1.08. Cooray (1999) finds a different slope of 0.66 ± 0.06 using the luminosity in the 2–10 keV band. The reason for the difference is probably that gas masses within a fixed radius of 0.5 Mpc were used in the analysis by Cooray.

The gas mass fraction shows a marginal trend to increase with luminosity (see Fig. 8c, again the gas mass fraction outlier AXJ2019+112 is excluded). This trend is mainly caused by the very low and very high luminosity clusters Cl0500-24 and RXJ1347-1145. The other clusters would be perfectly consistent with a horizontal line. As the linear correlation coefficient predicts a high probability for a correlation between the luminosity and the gas mass fraction, we try to fit these data, but the large error on the slope reflects the consistency with a constant gas mass fraction

$$f_{gas,500} = M_{gas,500}/M_{tot,500} = 0.13 \, L_{X,bol}^{(0.29 \pm 0.86)}, \tag{14}$$

(with $L_{X,bol}$ in units of 10^{45} erg/s). For comparison, in a nearby sample with a much larger range of luminosities Jones & Forman (1999) find an increase of the gas mass with luminosity.

Fig. 8d shows the iron mass versus luminosity. There might be a marginal trend of increasing iron mass with luminosity, but again the error bars on the iron mass are too large to get any significant result.

The relative gas extent E (Fig. 8e) – expressed as the ratio of gas mass fraction at r_{500} and $0.5 \times r_{500}$ – shows a less pronounced correlation with luminosity than with total mass (Fig. 2d) or with temperature (Fig. 5c). A fit excluding AXJ2019+112 yields

$$E = f_{gas}(r_{500})/f_{gas}(r_{500/2}) = 87 \, L_{X,bol}^{(-0.091 \pm 0.063)}, \tag{15}$$

with $L_{X,bol}$ in units of 10^{45} erg/s.
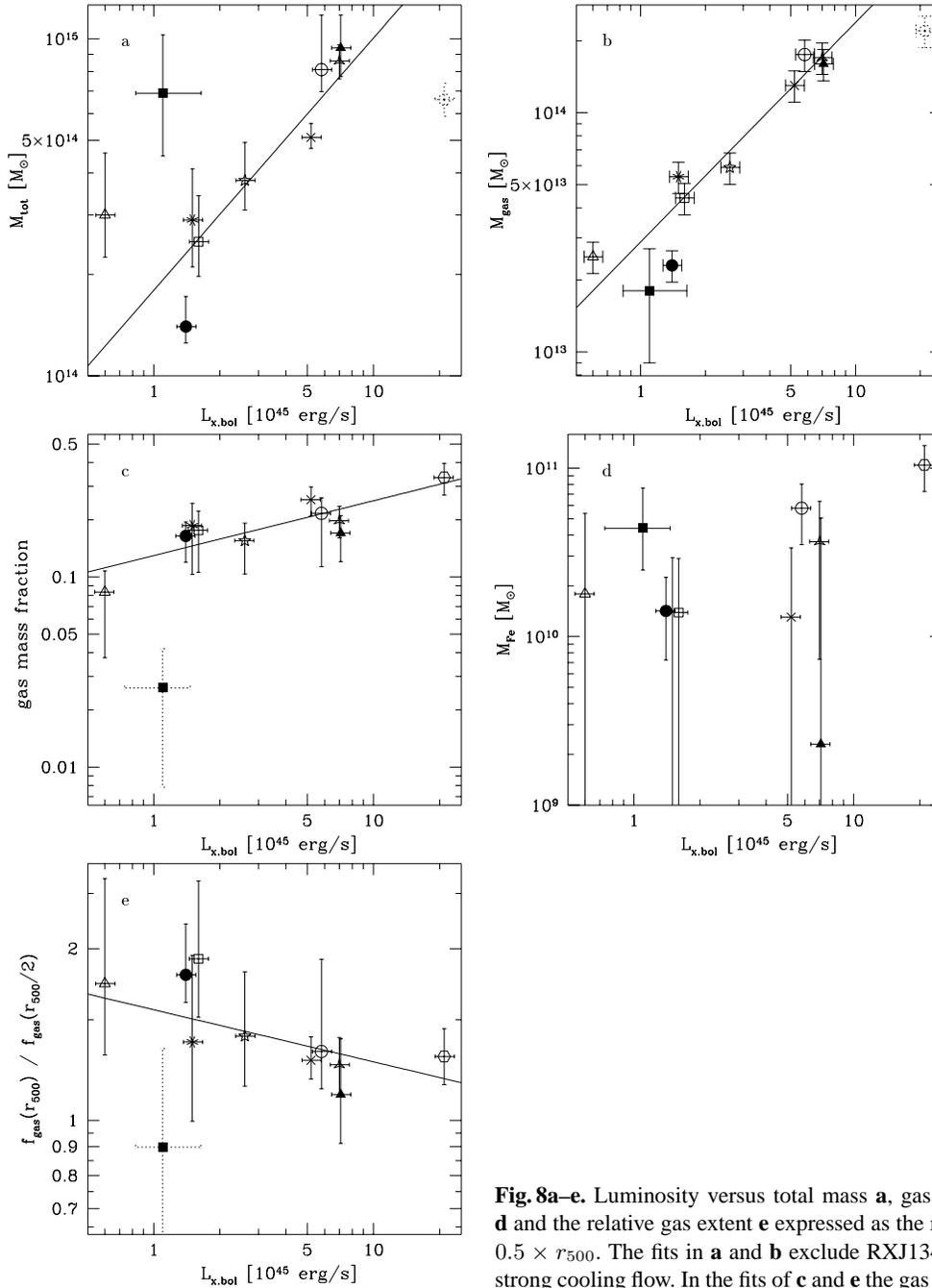
Fig. 8a–e. Luminosity versus total mass **a**, gas mass **b**, gas mass fraction **c**, iron mass **d** and the relative gas extent **e** expressed as the ratio of the gas mass fraction at r_{500} and $0.5 \times r_{500}$. The fits in **a** and **b** exclude RXJ1347-1145 (dotted hexagon) because of its strong cooling flow. In the fits of **c** and **e** the gas mass outlier AXJ2019+112 is excluded.

3.4. β-model parameters

Neumann & Arnaud (1999) found a correlation between the fit parameters of the β model – the core radius r_c and the slope β – when normalising the core radius. They normalised their core radii to r_{200}. As the X-ray emission of distant clusters cannot be traced out to such large radii we normalised the core radii to r_{500} (see Fig. 9a).

Obviously, there is also a correlation between the core radius r_c and the slope β in distant clusters. The error bars in Fig. 9a seem large and are somewhat misleading. The error range is not the whole rectangle defined by these error bars, but more like a very elongated ellipse from the lower left corner to the upper right corner.

A fit with a power law taking into account the errors in both parameters yields

$$\beta = 0.80 \left(\frac{r_c}{r_{500}} \right)^{(0.13 \pm 0.04)} . \tag{16}$$

For comparison we plot in Fig. 9a also the fit curve by Neumann & Arnaud (1999) for nearby clusters after converting their normalising radius with a factor 0.63 to ours. Due to the large error bars we cannot determine which fit function is the better one.
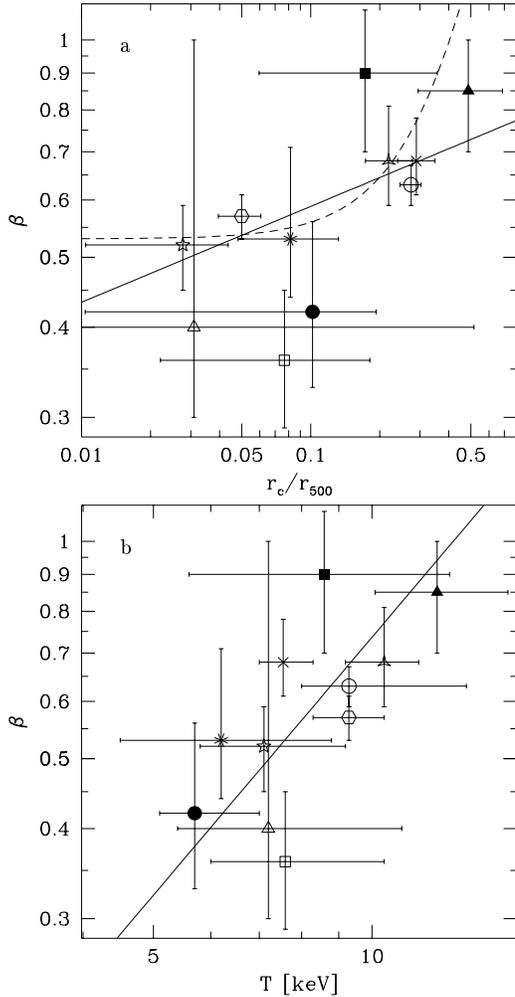
Fig. 9. a Core radius – β relation. The dashed line is the best fit core radius – β relation by Neumann & Arnaud (1999). The full line is a fit with a power law taking into account the errors in both parameters. **b** Temperature – β relation.

Both come close to all clusters with small error bars and seem to fit the data equally well.

In Fig. 9b we show the dependence of β on the temperature. There is a trend to find larger β values for larger temperatures as was also found for more nearby clusters (Mohr & Evrard 1997; Arnaud & Evrard 1999; Jones & Forman 1999). We find

$$\beta = 0.048\, T^{(1.2\pm0.5)}, \tag{17}$$

with T in keV.

4. Summary and conclusions

Using ROSAT and ASCA results of distant clusters we derive bolometric luminosities, total masses, gas masses, gas mass fractions and iron masses. We compare these with directly measured quantities: temperature, metallicity, redshift, core radius and the slope parameter β. We find clear positive correlations between the following quantities:

- total mass
- gas mass
- temperature
- luminosity
- r_{500}
- β
- normalised core radius.

and a negative correlation of the

- relative gas extent

with the other quantities. No correlations are found between the gas mass fraction and the other quantities.

All relations are in agreement within the errors with relations found in nearby cluster samples, i.e. consistent with no evolution, although we find for some relations slightly different slopes, but the differences are not significant because of the large uncertainties. Furthermore, we find no trend with redshift in the quantities themselves.

A low Ω is required to explain the high gas mass fraction of $\langle fgas \rangle = 0.18$, because in an $\Omega = 1$ universe this value is much higher than the baryon fraction predicted by primordial nucleosynthesis. A low Ω is also favoured by the fact that we see no evolution in temperature or mass with redshift, because in $\Omega = 1$ universe one would expect on average cooler clusters at high redshift (Oukbir & Blanchard 1992). Furthermore, as the changes in the luminosity temperature relation are expected to be larger in an high Ω universe (Eke et al. 1998), our results are consistent also here with low Ω, but $\Omega = 1$ can not be excluded because of the large uncertainties. Summarising, these quantities point towards a low Ω universe, but for final conclusions they need to be measured with higher accuracy.

While some relations have been known for a long time from nearby samples, e.g. the luminosity-temperature relation (Mushotzky 1984) or the increase of the gas mass fraction with radius, others are not well known yet: a negative correlation of the relative gas extent and cluster mass or temperature and a tight correlation between the bolometric luminosity and gas mass. Both give interesting insights into cluster structure and formation.

The relative gas extent E, defined as the ratio of the gas mass fraction at r_{500} and $0.5 \times r_{500}$, is a measure of how fast the gas mass fraction is increasing with radius and as such a measure of how extended the gas distribution is with respect to the dark matter distribution. Large values of the ratio E – corresponding to very extended gas distribution – are found in the clusters with low mass and low temperature, while low ratios E of almost unity – corresponding to similar distributions in gas and dark matter – are found in massive and hot clusters. This can have different reasons. One possibility is that it hints to physical processes in the gas, which are assumed to be responsible for the increase of gas mass fraction with radius (e.g. Metzler & Evrard 1997; Cavaliere et al. 1998a). If gas is placed artificially into a model cluster potential in hydrostatic equilibrium the distributions of gas and dark matter have the same slope at radii larger than the core radius (Navarro et al. 1996), therefore one

would expect a priori a ratio $E \approx 1$. It might be that this additional heat input affects low mass clusters more that massive clusters, so that a massive cluster can maintain a ratio $E = 1$ while in the smaller clusters the gas is becoming more and more extended. Another possibility is that this relation points to some other hidden correlation. For example, if the clusters have temperature profiles declining with radius, with our assumption of isothermality we are underestimating E. If e.g. the temperature profiles in less massive cluster were steeper than in more massive clusters we would also expect a gradient in E with mass. This is just an example to show how different correlations could be connected. In this case it is probably not an effect of temperature profiles, because Markevitch et al. (1998) found the same temperature gradient in hot and cool clusters. This dependence of the relative gas extent E should be tested in nearby clusters, where the masses can be measured with higher accuracy.

We find large variations in the gas mass fraction, similar to the results of nearby clusters (Reiprich 1998; Ettori & Fabian 1999). These large variations, which span an order of magnitude, have some implications on cluster formation. If all the clusters had originally the same small gas mass fraction and all the differences came later by different amounts of gas released by the cluster galaxies, larger metallicities in clusters with high gas mass fraction would be expected. But this is not observed. Therefore the difference must be caused at least partially by the primordial distribution of baryonic and non-baryonic matter.

The tight correlation of gas mass and bolometric luminosity gives a hint that there is not a lot of clumpiness on small scales in the intra-cluster gas. If there would be different degrees of clumpiness one would expect a large scatter around the fit, because with the same amount of gas a clumpier medium produces more photons as the emission is proportional to the square of the density. Although a non-clumpy medium is implicitly assumed for the calculation of the gas mass, the fact that everything is consistent is an interesting result. It confirms results found by the comparison of X-ray data and Sunyaev-Zel'dovich measurements. As the two measurements have different dependencies on the gas density a large degree of clumpiness could be ruled out (e.g. Holzapfel et al. 1997).

Unfortunately, the errors in the metallicity measurement are very large (only half of clusters in the samples have metallicities non-consistent with zero). Hence, also the errors in the iron masses are very large, so that no definite conclusions about the metal injection into the intra-cluster medium and its time dependence can be drawn.

The comparison with other clusters shows that AXJ2019+112 is really an exceptional cluster. It is not only the most distant cluster in the sample, but it is also the only cluster found indirectly by the gravitational lensing effect. It has by far the highest metallicity, the lowest gas mass fraction and the lowest relative gas extent. Unfortunately, the morphological parameters could not be very well constrained from the ROSAT/HRI observation because only about 80 source counts were detected (Hattori et al. 1997). Therefore, we test what effects a small change of the morphological parameters would have on the masses. Assuming the slope

β was 0.6 (instead of the best fit value $\beta = 0.9$), one finds a total mass of $M_{tot,\beta=0.6} = 3.6 \times 10^{14} M_\odot$ and a gas mass of $M_{gas,\beta=0.6} = 0.32 \times 10^{14} M_\odot$. Comparing these with the masses for $\beta = 0.9$, $M_{tot,\beta=0.9} = 6.9 \times 10^{14} M_\odot$ and $M_{gas,\beta=0.9} = 0.18 \times 10^{14} M_\odot$, and with the masses expected from the luminosity – mass relations, $M_{tot,exp} = 2.0 \times 10^{14} M_\odot$ and $M_{gas,exp} = 0.28 \times 10^{14} M_\odot$, one sees that with $\beta = 0.6$ the masses are already much less exceptional. Also the gas mass fraction with 9% would be much closer to the expected values. Only the relative gas extent $E_{\beta=0.6} = 0.85$ would still be unexplainable. Further investigation of this interesting cluster is definitely necessary.

In this work we showed that important relations in distant clusters can be found by a combination of ROSAT and ASCA data. But we also showed that there are limitations in these data for distant clusters. We could not find any significant evidence for evolution. But on the other hand, due to the large uncertainties in the mass determination, in the temperature and the metallicity measurements we could not rule out differences between distant and nearby cluster. We are expecting huge improvements of the situation with the upcoming X-ray missions XMM, CHANDRA and ASTRO-E. In terms of cosmology with distant clusters clearly two ways are to be followed. (1) The cluster parameters used in this work need to be measured with much better accuracy for clusters with redshifts considered here. In particular, a more accurate temperature measurement is essential for the determination of the total mass and the gas mass fraction. Metallicities with much smaller errors are required to explain the origin of the intra-cluster medium. (2) As the evolutionary effects become stronger with larger redshifts it is crucial to find clusters at very high redshifts ($z \gtrsim 1$) like first studies have shown is possible (e.g. Dickinson 1996; Deltorn et al. 1997; Carilli et al. 1998).

References

Allen S.W., Fabian A.C., 1998, MNRAS 297, L57
Arnaud M., Evrard A.E., 1999, MNRAS 305, 631
Bower R.G., 1997, MNRAS 288, 355
Burke D.J., Collins C.A., Sharples R.M., et al., 1997, ApJ 488, L83
Carilli C.L., Harris D.E., Pentericci L., et al., 1998, ApJ 494, L143
Cavaliere A., Fusco-Femiano R., 1976, A&A 49, 137
Cavaliere A., Menci N., Tozzi P. 1998a, ApJ 501, 493
Cavaliere A., Menci N., Tozzi P. 1998b, astro-ph/9810498
Cen R., Ostriker J.P., 1994, ApJ 429, 4
Cooray A.R., 1999, astro-ph/9905095
David L.P., Jones C., Forman W., 1995, ApJ 445, 578
Deltorn J.-M., Le Fèvre O., Crampton D., Dickinson M., 1997, ApJ 483, L21
Dickinson M., 1996, astro-ph/9612178
Donahue M., 1996, ApJ 468, 79

Donahue M., Voit G.M., Gioia I., et al., 1998, ApJ 502, 550

Eke V.R., Navarro J.F., Frenk C.S., 1998, ApJ 503, 569

Ettori S., Fabian A.C., 1999, astro-ph/9901304

Evrard A.E., Metzler C.A., Navarro J.F., 1996, ApJ 469, 494

Fabian A.C., Crawford C.S., Edge A.C., Mushotzky R.F., 1994, MN-RAS 267, 779

Fukazawa Y., Makishima K., Tamura T., et al., 1998, PASJ 50, 187

Furuzawa A., Tawara Y., Kunieda H., et al., 1998, ApJ 504, 35

Gioia I.M., Henry J.P., Mullis C.R., Ebeling H., Wolter A., 1999, AJ, in press, astro-ph/9902277

Grupe D., Beuermann K., Thomas H.-C., Mannheim K., Fink H.H., 1998, A&A 330, 25

Guzzo L., Böhringer H., Schuecker P., et al., 1999, ESO Messenger, in press

Hattori M., Ikebe Y., Asaoka I., et al., 1997, Nat 388, 146

Hattori M., Matuzawa H., Morikawa K., et al., 1998, ApJ 503, 593

Henry J.P., 1997, ApJ 489, L1

Hjorth J., Oukbir J., van Kampen E., 1998, MNRAS 298, L1

Holzapfel W.L., Arnaud M., Ade P.A.R., et al., 1997, ApJ 480, 449

Horner D.J., Mushotzky R.F., Scharf C.A., 1999, astro-ph/9902151

Hughes J.P., Birkinshaw M., 1998, ApJ 501, 1

Jones C., Forman W., 1984, AJ 276, 38

Jones C., Forman W., 1999, ApJ 511, 65

Kaiser N., 1986, MNRAS 222, 323

Markevitch M., 1998, ApJ 504, 27

Markevitch M., Forman W.R., Sarazin C.L., Vikhlinin A., 1998, ApJ 503, 77

Martinelli A., Matteucci F., Colafrancesco S., 1999, astro-ph/9905138

Metzler C.A., Evrard A.E., 1997, astro-ph/9710324

Mo H.J., Jing Y.P., White S.D.M., 1996, MNRAS 282, 1096

Mohr J.J., Evrard A.E., 1997, ApJ 491, 38

Mohr J.J., Mathiesen B., Evrard A.E., 1999, astro-ph/9901281

Mushotzky R.F., 1984, Phys. Scr. T7, 157

Mushotzky R.F., Loewenstein M., 1997, ApJ 481, L63

Mushotzky R.F., Scharf C.A., 1997, ApJ 482, L13

Navarro J.F., Frenk C.S., White S.D.M., 1996, ApJ 462, 563

Neumann D.M., 1999, ApJ in press, astro-ph/9902035

Neumann D.M., Arnaud M., 1999, astro-ph/9901092

Neumann D.M., Böhringer H. 1997, MNRAS 289, 123

Neumann D.M., Schindler S., 1999, in preparation

Ota N., Mitsuda K., Fukazawa Y., 1998, ApJ 495, 170

Oukbir J., Blanchard A., 1992, A&A 262, L21

Oukbir J., Blanchard A., 1997, A&A 317, 1

Reiprich T.H., 1998, Diploma Thesis, Ludwig-Maximilians-Universität München

Reiprich T.H., Böhringer H., 1999, In: Inoue H., Ohashi T., Takahashi T. (eds.) Proceedings of the 4th ASCA Symposium on Heating and Acceleration in the Universe. Held in Tokyo, Japan, in press

Sadat R., Blanchard A., Oukbir J., 1998, A&A 329, 21

Scharf C.A., Mushotzky R.F., 1997, ApJ 485, L65

Schindler S., 1996, A&A 305, 756

Schindler S., Wambsganss J., 1996, A&A 313, 113

Schindler S., Wambsganss J., 1997, A&A 322, 66

Schindler S., Hattori M., Neumann D.M., Böhringer H., 1997, A&A 317, 646

Schindler S., Belloni P., Ikebe Y., et al., 1998, A&A 338, 843

Tanaka Y., Inoue H., Holt S.S., 1994, PASJ 46, L39

Trümper J., 1983, Adv. Space Res. 2, 142

Tsuru T., Koyama K., Hughes J.P., et al., 1996, In: Yamashita K., Watanabe T. (eds.) Proceedings of the 11th Colloquium on UV and X-ray Spectroscopy of Astrophysical and Laboratory Plasmas. Held in Nagoya, Japan, Universal Academic Press, Tokyo, p. 375

Tsuru T.G., Matsumoto H., Koyama K., et al., 1997, astro-ph/9711353

Voit G.M., Donahue M., 1998, ApJ 500, L111

Wu X.-P., Xue Y.-J., Fang L.-Z., 1999, astro-ph/9905106